

## Deactivation of Mesoporous Titanosilicate-supported $\text{WO}_3$ Catalyst for Metathesis of Butene to Propene by Coke

Derun Hua<sup>1\*</sup>, Zheng Zhou<sup>2</sup>, Jian Li<sup>1</sup>, Yongrong Xie<sup>1</sup> and Xinning Lu<sup>1</sup>

<sup>1</sup>Chemical Institute of Chemical Industry, Gannan Normal University, Jingxi, 341000, China

<sup>2</sup>Natural Gas Processing Plant of Sinopec Zhongyuan Oilfield Branch, Henan, 457000, China

### Abstract

Catalyst deactivation by coke was studied during metathesis of butene to propene on the  $\text{WO}_3/\text{MTS-9}$  catalyst. Characterization results of the coked catalyst showed that the pore volume, pore size, and specific surface area of the catalyst decreased significantly for coke; the coke amount in larger pore of catalyst was higher than that in smaller pores of the catalyst. Coke resulted in the decrease of the acidic amount and the activity of catalyst. The component of carbon deposits was aromatic-olefin compounds.

**Keywords:** Deactivation; Metathesis; Coke; MTS-9

### Introduction

Olefin metathesis reported in the 1960s by Banks is an organic reaction that entails the redistribution of fragments of alkenes (olefins) by the scission and regeneration of carbon-carbon double bonds [1]. Olefin metathesis has been used as an important way for olefin conversion and offers a path to convert low value olefins into high-value olefins, such as propene, ethene [2-5], short-chain olefin to long-chain olefin [6,7], and butene to propene [8,9]. Supported  $\text{WO}_3$  catalysts are known to catalyze the reaction [8-11] and are currently applied industrially for heterogeneous catalysis metathesis reactions. Now, many studies have been carried out to improve performance of supported  $\text{WO}_3$  catalysts [12,13]. Many factors, such as the method of catalyst preparation, reaction conditions, structure of the support and so on, affect catalytic activity. Debecker et al. [14] and Debecker et al. [15] prepared  $\text{WO}_3$ -based metathesis catalyst with high catalytic performance and shorter induction period by the one-step Sol-gel process. One-pot sol-gel catalysts perform better than corresponding impregnated catalysts, which were attributed to fact that the sol-gel method can control well on the final composition and textures of catalyst. Piyasan et al. [16] found that  $\text{WO}_3/\text{SiO}_2$  catalysts treated by NaOH held a shorter induction period and low coke at the same metathesis activity. Piyasan et al. [17] suggested that silica-supported tungsten catalysts mixed with micro- and nano-sized  $\text{SiO}_2$  excess support favored to form isolated surface tetrahedral tungsten oxide species. Phatanasri et al. [18] found that the calcination temperature markedly affected physico-chemical properties of the catalysts, particularly the active species of  $\text{WO}_3/\text{SiO}_2$  catalysts. Khattaf et al. [19] investigated MCM-41- and SBA-15-supported tungsten catalyst. Supported oxide catalysts and mesoporous catalysts have been reviewed recently [20,21].

As heterogeneous catalysis, catalysts deactivation often occurs during olefin-metathesis reactions due to carbonaceous species formed on catalyst surface. The carbonaceous species deposit on the surface of catalyst, and results in deactivation of the catalyst. The mechanism for catalyst deactivation is complex. The causes of deactivation are various, such as poisoning, valence change of active sites, and active-site coverage [22]. For different types of catalysts employed to olefin-metathesis reactions, their deactivation reasons are different. For Re-supported catalysts, deactivation results from poisoning, and poison are adsorbed strongly on the surface of catalyst and hinder reactant to access the active sites [23]. For Mo-supported catalyst, the deep-reduction of Mo species may be the main reason for its deactivation during metathesis [24]. For the tungsten catalytic system, high reaction

temperatures (300–500°C) have to be used in order to achieve high metathesis activity and avoid poisoning [25], but coke is easy to form at a high temperature and high acid, and deposits on the surface of catalyst [16,26]. In the last few years, a large amount of investigations have been undertaken to study coke deposits (location and total amount) and to obtain information regarding the deactivation mechanism and regeneration. Moodley [27] investigated the effect of the coke amount on catalytic activity and the coking location, and found that 2-Pentanone was the most effective inhibitor for coking, and the location of coke deposition is a more important factor than the coke amount. In the case of alkene metathesis, deep-reduction may result in deactivation [28]. Besides, it was found that water and polar solvents are useful to coke retardation [25,29] at a high temperature. Unfortunately, the coking location and the structure of carbon species are not clear.

In this study, the optimized 8.0 wt.% W supported on MTS-9 was used as the catalyst for metathesis of butene to propene. The deactivated catalyst was characterized, and regenerated by treating at 500°C in atmosphere.  $\text{N}_2$  adsorption-desorption was used to detect pore size and pore volume of the catalyst before and after reaction.  $^{13}\text{C-NMR}$  and UV-Raman are used to investigate the nature of the carbonaceous species. STEM (scanning transmission electron microscopy) and EFTEM (energy filtered transmission electron microscopy) are used to monitor the coked location.

### Experimental

#### Preparation of catalyst

MTS-9 was hydrothermally synthesized in a two-step procedure as given in the literature. First, precursors containing titanosilicate (TS-1) nanoclusters were prepared. Second, the preformed precursors were assembled with triblock copolymers in a strong acid medium

**\*Corresponding author:** Derun Hua, Chemical Institute of Chemical Industry, Gannan Normal University, Jingxi, 341000, China, Tel: +8607978973396; E-mail: dr\_hua2011@sina.com

Received March 02, 2016; Accepted March 08, 2016; Published March 15, 2016

**Citation:** Hua D, Zhou Z, Li J, Xie Y, Lu X (2016) Deactivation of Mesoporous Titanosilicate-supported  $\text{WO}_3$  Catalyst for Metathesis of Butene to Propene by Coke. J Thermodyn Catal 7: 162. doi:10.4172/2160-7544.1000162

**Copyright:** © 2016 Hua D, et al. This is an open-access article distributed under the terms of the Creative Commons Attribution License, which permits unrestricted use, distribution, and reproduction in any medium, provided the original author and source are credited.

(pH<1) [30,31]. WO<sub>3</sub>/MTS-9 catalysts with tungsten loading (8.0 wt.%) was prepared by a wet impregnation method with water solutions of ammonium metatungstate. The impregnated product was dried at 80°C for 12 h; then the catalyst was thermally treated at 550°C for 4 h in a temperature programmed furnace (1 K/min) [32]. Texture of support and catalyst was listed in Table 1.

### Characterization of catalyst

N<sub>2</sub> adsorption-desorption isotherms at -196°C were recorded with a Micromeritics ASAP 2010 automatic sorption analyzer. The BET surface areas were calculated from the desorption isotherms in the relative pressure range of  $P/P_0=0.01\sim 1.0$ . UV-Raman spectra were obtained on a HR800 UV-Raman Spectrograph (Horiba Jobin Yvon Company, France). The 44.0 nm line from a He-Cd was used as the excitation source, and the spectrum resolution was estimated to be 4.0 cm<sup>-1</sup>. STEM and EFTEM images were obtained with a Tecnai G2 F20 Super-twin (FEI Company). A <sup>13</sup>C-NMR study was conducted on a Bruker Avance DSX400 NMR spectrometer at a frequency of 100.6 MHz. The peaks were referenced to tetramethylsilane (TMS) as an external standard. The spinning rate was 3-4 kHz. Temperature programmed desorption (TPD) was conducted by ramping to 500°C at 10°C/min and NH<sub>3</sub> (m/e=16) in the effluent was detected and recorded as a function of temperature by a thermal conductivity detector (TCD) (BJGC, GSD301, China). All products were analyzed using a gas chromatograph equipped with a flame ionization detector (FID) and a 50 m PONA capillary column. The acid sites amount and strength distribution of samples were determined by a temperature-programmed desorption of ammonia (NH<sub>3</sub>-TPD). The ammonia in the effluent gas was detected by a TCD detector, and then adsorbed with 0.02 mol/L HCl solution. The total acidic amount was determined by back-titrating the HCl solution using 0.01 mol/L NaOH solution, and bromocresol green/methyl red as indicator.

### Reaction

The metathesis reaction of butene (1-butene and 2-butene) was carried out in a downflow fixed bed stainless steel reactor (i.d., 10 mm) with 0.375 g catalyst. The C<sub>4</sub> stream, which are from MTBE chemistry in Shanghai and compose of 2-butene (ca. 78%, wt/wt) and butane (18%), was treated through BASF adsorbents Selexsorb CD and COS to remove oxygenated organic compounds (methanol, MTBE) and other trace contaminants, which can cause catalyst deactivation. Before the introduction of C<sub>4</sub> stream into the reactor, the catalyst was pretreated in situ with a N<sub>2</sub> and H<sub>2</sub> (2%, vol/vol) mixture flow for 30 min at 420°C and atmospheric pressure. The weight hour space velocity (WHSV) of the metathesis reaction was 3.2 h<sup>-1</sup>.

### Results and Discussion

After 320 h, the conversion of butene decreases from ca. 50% to ca. 25% (see Figure 1). The catalyst was discharged, then characterized to study the mechanism of coking and the deactivation reason. The N<sub>2</sub> adsorption-desorption isotherm of the fresh and spent catalysts is compared (see Figure 2a). It is found that the spent catalyst had a smaller pore volume than the fresh catalyst, suggesting that pore blockage occurs for carbon deposition. The texture of the catalyst is listed in Table 1. The distribution of the pore size of the spent catalyst is presented in Figure 2b. The Figure 2b shows that carbonaceous deposit filled the pores of the catalyst. The carbon deposit amount in the larger pores is higher than that in the smaller pores. Coking depends mainly on feedstock, temperature, catalyst acidity and pore size [33]. At the same conditions, carbon deposit depends on the texture of the catalyst. The available space was larger. The coking amount was greater.

The scanning transmission electron microscopy (STEM) images of the spent and fresh catalyst are shown in Figure 3. The lightest regions (dashed circle) show the crystallites of tungsten oxide on the silica support. The lighter regions (dashed rectangle) show the surface tungsten interacting with support. The darkest regions (solid rectangle) show the support. The pore fingerprint of the fresh catalyst is clear in Figure 3A, but that of the spent catalyst is not found in Figure 3B.

Sample	Pore diameter (nm)	Total pore volume (cm <sup>3</sup> /g)	Micropore volume (cm <sup>3</sup> /g)	Mesopore surface area (m <sup>2</sup> /g)
MTS-9	6.75	0.987	0.048	489.1
Catalyst	6.346	0.7125	0.0205	436.5
Spent catalyst	5.84	0.2944	0.002508	201.6

Table 1: Textural features of support and catalyst.

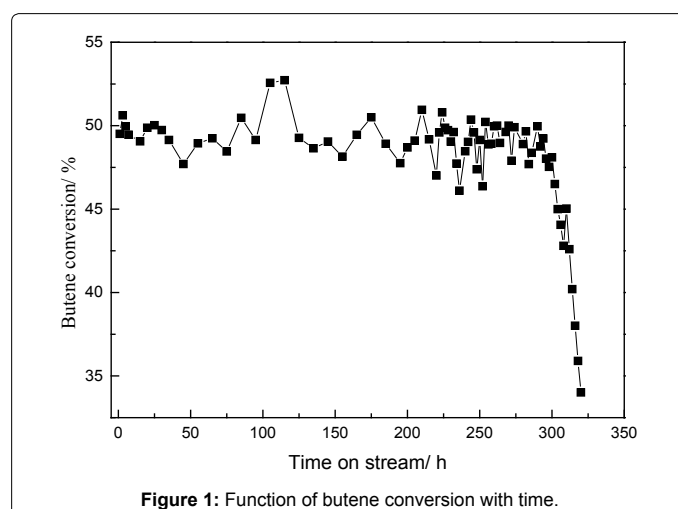


Figure 1: Function of butene conversion with time.

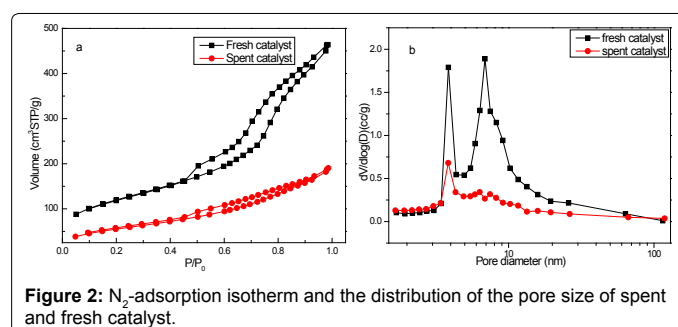


Figure 2: N<sub>2</sub>-adsorption isotherm and the distribution of the pore size of spent and fresh catalyst.

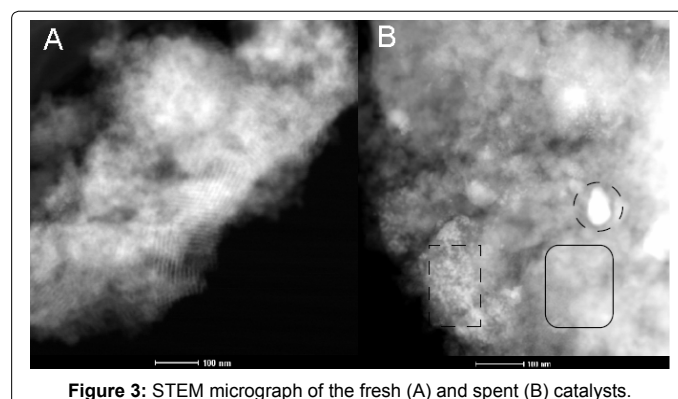


Figure 3: STEM micrograph of the fresh (A) and spent (B) catalysts.

The EFTEM technique is used to acquire the location of coke on the WO<sub>3</sub>/MTS-9 catalyst. The carbon map of the catalyst is shown in Figure 4A; the tungsten map of the catalyst is shown in Figure 4B. In Figure 4C, red regions are carbon maps, and the blue regions are tungsten maps. The carbon maps in Figure 4C show that all the carbon (red region) surrounds the tungsten oxide (blue region in the centre), that is, carbon deposition occurs around the tungsten, and tungsten is not covered by carbon. Effect of coke on the acidic amount of catalysts is listed in Table 2. A comparison of the acidic amount of catalysts, it is found that the acidic amount of the fresh catalyst is more than that of support, which indicates that the formation of new acidic sites is resulted from the interaction of tungsten and support. However, the acidic amount of the spent catalyst is less than that of the fresh catalyst, even is less than that of support, which indicates the acidic sites are covered by coke. Namely, the coking location is at the acidic sites.

We attempt to study the composition of coke by <sup>13</sup>C-NMR (Figure 5). As shown in Figure 5, the resonance line of the spent catalyst is wide, indicating that condensed carbonaceous compounds are present [34]. Besides the above information, the <sup>13</sup>C-NMR spectrum of spent catalyst exhibits two distinct groups of resonance lines, which are assigned to aliphatic (0-50 ppm) and aromatic (100-150 ppm) carbons. The resonance peak at 25 ppm is attributed to methyl group attached to aromatic ring [35]. The resonance peak at 47 ppm is assigned to methyl-substituted cyclopentenyl carbocation, which was reported as intermediates in the formation of aromatic hydrocarbon [36]. The resonance peak at 127 ppm corresponds to aromatic C-H bonds or olefin [37,38]. Since the operation temperature is above 350°C, coke components are polyaromatic regardless of other conditions [33].

Figure 6 shows the ultraviolet Raman spectrum of the fresh and spent catalysts. For the fresh catalyst, Raman spectrum consisted mainly of bands at 995 and 1087 cm<sup>-1</sup>. Raman bands of 1087 and 995 cm<sup>-1</sup> are the characteristic of surface tungsten oxide species (active species). Bands at 1087 and 995 cm<sup>-1</sup> corresponded to the stretching vibration mode of the terminal bond of isolated surface tungsten oxide species and surface poly tungsten, respectively [39,40]. On the spent catalyst, the strong bands of 1396 and 1610 cm<sup>-1</sup> were observed. It was interesting that bands of 1087 and 995 cm<sup>-1</sup> disappear or become weak. This is because the bands due to carbon are more intense and flatten Raman bands at 1087 and 995 cm<sup>-1</sup>.

Raman bands assignments for vibrations in the region from 1000 to 1650 cm<sup>-1</sup> are listed in Table 3 [41]. Compared Table 2 with the UV-Raman spectra of the spent catalyst in Figure 6, bands at 1396 and 1610 cm<sup>-1</sup> correspond to the ring stretches of poly aromatic species. Based on the results of <sup>13</sup>C-NMR (Figure 5) and UV-Raman spectra (Figure

Catalysts	WO <sub>3</sub>	MTS-9	Fresh catalyst	Spent catalyst
Acidic amount (mmol/g)	0	0.188	0.261	0.157

Table 2: The acidic amount of catalysts.

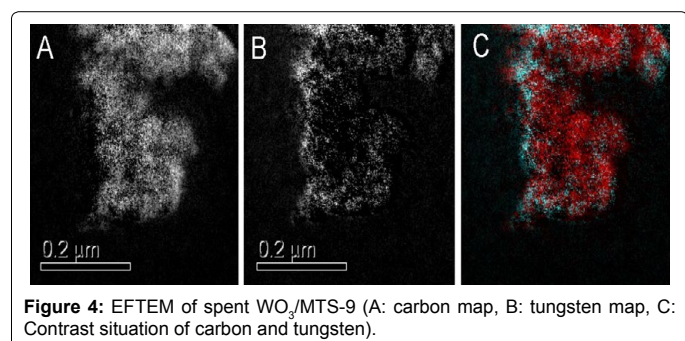


Figure 4: EFTEM of spent WO<sub>3</sub>/MTS-9 (A: carbon map, B: tungsten map, C: Contrast situation of carbon and tungsten).

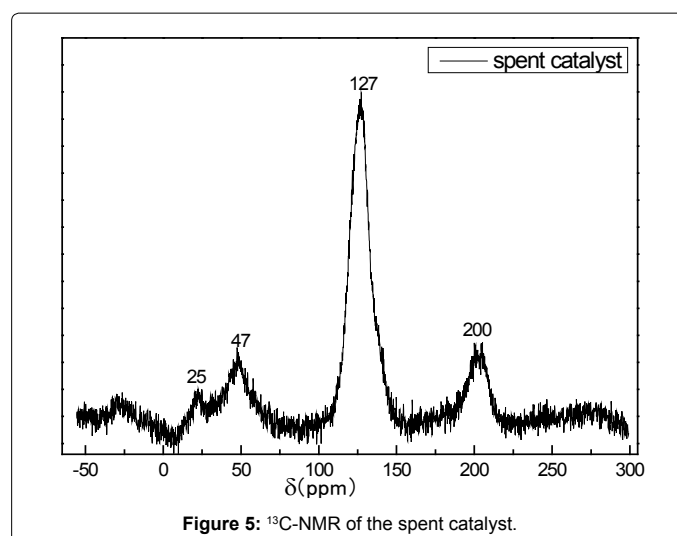


Figure 5: <sup>13</sup>C-NMR of the spent catalyst.

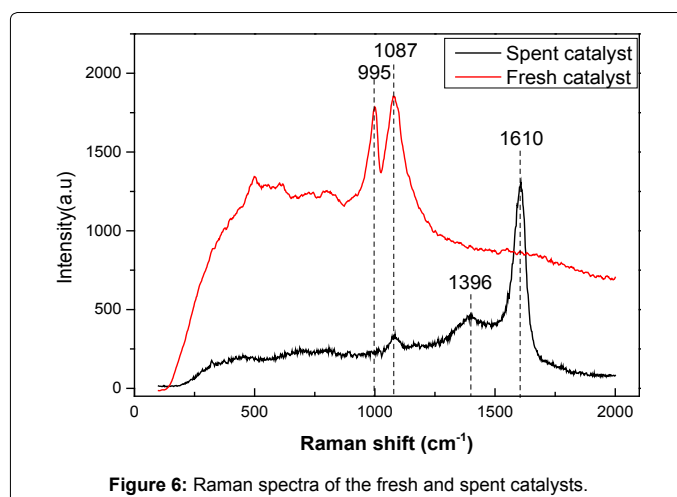


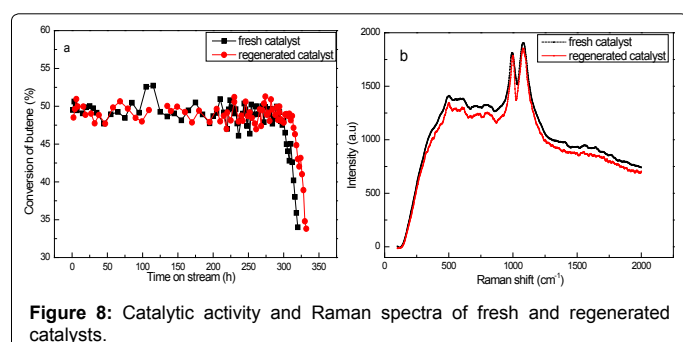
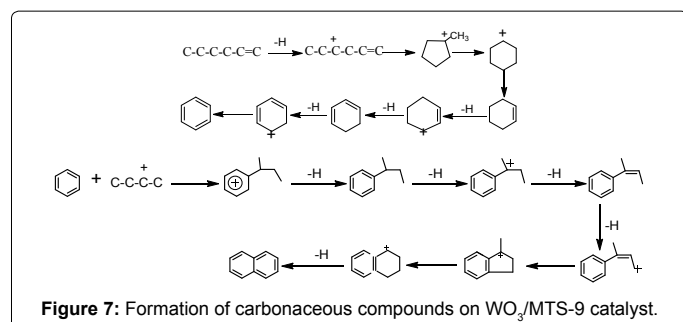
Figure 6: Raman spectra of the fresh and spent catalysts.

6) of the spent catalyst, it is definite that the component of coke is poly aromatic species.

The UV-Raman spectrum of the spent catalyst is compared with the UV-Raman spectra of a series of polyaromatic compounds, such as naphthalene, phenanthrene, anthracene, fluorene, pyrene, pentacene, and coronene. UV-Raman measurements of these compounds have been reported previously by Chua and Stair [41,42], and Johnson [29]. By contrast, the spectrum of carbon deposits on WO<sub>3</sub>/MTS-9 is similar to that of the chain-like polyaromatic compounds, such as naphthalene and pentacene.

The <sup>13</sup>C-NMR and UV-Raman spectrum provides some evidence for coke configuration. The formation of coke molecules includes condensation, hydrogen transfer and dehydrogenation processes. So the following reaction scheme (Figure 7) can be proposed to explain the formation of coke molecules. Benzenic compounds are formed through the scheme of aromatization on the WO<sub>3</sub>/MTS-9 catalyst.

The deactivated catalyst was regenerated at 500°C under air flow, and the performance of the fresh and regenerated catalyst was compared, as shown in Figure 8a. It can be seen that the activity of the regenerated catalyst is comparable to that of the fresh one, suggesting that the regeneration of the deactivated catalyst is feasible. Figure 8b shows Raman spectra of the regenerated and fresh catalyst.



Raman shift (cm <sup>-1</sup> )	Raman band assignments
1605-1615	Ring stretches of polyaromatic species
1360-1410	Ring stretches of polyaromatic species
1200-1210	C-C stretches of polyaromatic species
1545-1550	C=C stretches of conjugated olefins
1483	In-phase C=C stretch of cyclopentadienyl species

**Table 3:** Raman band assignments.

In comparison with Raman spectra of the fresh catalyst, there are no changes. So the fresh and regenerated catalyst holds the same activity.

## Conclusions

According to results of BET, EFTEM and Raman, deactivation of WO<sub>3</sub>/MTS-9 catalyst is attributed to the pore blockage. Coke results in the decrease of the acidic amount of the spent catalyst. According to our experiments, the coking location successfully determined is on the support and the active sites rather than the tungsten oxide crystallite and results indicate that the decrease of catalytic activity results from the coverage of the active sites. The deposited carbon is aromatic compounds, which the process of formation is speculated. Moreover, the deactivated catalyst may be regenerated at 500°C under air flow, and the regenerated catalyst holds as high activity as the fresh catalyst.

## Acknowledgements

The authors are grateful for the financial supports from the National Natural Science Foundation of China (No. 21466001).

## References

- Banks R, Bailey G (1964) Olefin Disproportionation. A New Catalytic Process. *Ind Eng Chem Prod Res Dev* 3: 170-173.
- Basur AG, Patwardhan SR, Vyas SN (1991) Propene metathesis over silica-supported tungsten oxide catalyst—Catalyst induction mechanism. *J Catal* 127: 86-95.
- Andreini A, MOL JC (1985) Journal of the Chemical Society, Faraday Transactions 1: Physical Chemistry in Condensed Phases. *J Chem Soc Faraday Trans I* 81: 1705-1714.
- Schrock RR (1999) Olefin metathesis by molybdenum imido alkylidene catalysts. *Tetrahedron* 55: 8141-8153.
- Andreini A, Xu XD, Mol JC (1986) Activity of Re<sub>2</sub>O<sub>7</sub>/SiO<sub>2</sub>-Al<sub>2</sub>O<sub>3</sub> catalysts for propene metathesis and the influence of alkyltin promoters. *Appl Catal* 27: 31-40.
- Topka P, Balcar H, Rathouský J, Zilková N, Verpoort F, et al. (2006) Metathesis of 1-octene over MoO<sub>3</sub> supported on mesoporous molecular sieves: The influence of the support architecture. *Microporous and Mesoporous Mater* 96: 44-54.
- Aguado J, Escola J, Castro M, Paredes B (2005) Metathesis of 1-hexene over rhenium oxide supported on ordered mesoporous aluminas: comparison with Re<sub>2</sub>O<sub>7</sub>/γ-Al<sub>2</sub>O<sub>3</sub>. *Appl Catal A: General*, 284: 47-57.
- Zhang XJ, Huang W, Yang S, Sun LD, Zhang FY, et al. (2009) Psoriasis genome-wide association study identifies susceptibility variants within LCE gene cluster at 1q21. *Nat Genet* 41: 205-210.
- Aad G, Abbott B, Abdallah J, Abidinov O, Aben R, et al. (2015) Combined Measurement of the Higgs Boson Mass in pp Collisions at sqrt[s]=7 and 8 TeV with the ATLAS and CMS Experiments. *Phys Rev Lett* 114: 191803.
- Debecker DP, Stoyanova M, Rodemerck U, Colbeau-Justin F, Boissère C, et al. (2014) Aerosol route to nanostructured WO<sub>3</sub>-Al<sub>2</sub>O<sub>3</sub> metathesis catalysts: Toward higher propene yield. *Appl Catal A: General* 470: 458-466.
- Cheng Z, Lo CS (2012) Formation of Active Sites on WO<sub>3</sub> Catalysts: A Density Functional Theory Study of Olefin Metathesis. *ACS Catal* 2: 341-349.
- Huang S, Liu S, Zhu Q, Zhu X, Xin W, et al. (2007) The effect of calcination time on the activity of WO<sub>3</sub>/Al<sub>2</sub>O<sub>3</sub>/HY catalysts for the metathesis reaction between ethene and 2-butene. *Appl Catal A: General* 323: 94-103.
- Huang S, Liu S, Xin W, Bai J, Xie S, et al. (2005) Metathesis of ethene and 2-butene to propene on W/Al<sub>2</sub>O<sub>3</sub>-HY catalysts with different HY contents. *Mol Catal A: Chemical* 226: 61-68.
- Maksasithorn S, Praserttham P, Suriye K, Debecker DP (2015) Preparation of super-microporous WO<sub>3</sub>-SiO<sub>2</sub> olefin metathesis catalysts by the aerosol-assisted sol-gel process. *Microporous and Mesoporous Mater* 213: 125-133.
- Maksasithorn S, Praserttham P, Suriye K, Devillers M, Debecker DP, et al. (2014) WO<sub>3</sub>-based catalysts prepared by non-hydrolytic sol-gel for the production of propene by cross-metathesis of ethene and 2-butene. *Appl Catal A: General* 488: 200-207.
- Maksasithorn S, Debecker DP, Praserttham P, Panpranot J, Suriye K, et al. (2014) NaOH modified WO<sub>3</sub>/SiO<sub>2</sub> catalysts for propylene production from 2-butene and ethylene metathesis. *Chin J Catal* 35: 232-241.
- Limsangkass W, Praserttham P, Phatanasri S, Panpranot J, Chaemchuen S, et al. (2014) Influence of micro- and nano-sized SiO<sub>2</sub> excess support on the metathesis of ethylene and trans-2-butene to propylene over silica-supported tungsten catalysts. *React Kinet Mech Catal* 113: 225-240.
- Chaemchuen S, Phatanasri S, Verpoort F, Sae-ma N, Suriye K, et al. (2012) The structure-reactivity relationship for metathesis reaction between ethylene and 2-butene on WO<sub>3</sub>/SiO<sub>2</sub> catalysts calcinated at different temperatures. *Kinet Catal* 53: 247-252.
- Bhuiyan TI, Arudra P, Akhtar MN, Aitani AM, Abudawoud RH, et al. (2013) Metathesis of 2-butene to propylene over W-mesoporous molecular sieves: A comparative study between tungsten containing MCM-41 and SBA-15. *Appl Catal A: General*, 467: 224-234.
- Balcar H, Cejka J (2013) Mesoporous molecular sieves as advanced supports for olefin metathesis catalysts. *Coord Chem Rev* 257: 3107-3124.
- Lwin S, Wachs IE (2014) Olefin Metathesis by Supported Metal Oxide Catalysts. *ACS Catal* 4: 2505-2520.
- Guisnet M, Magnoux P Catal (1997) Deactivation by coking of zeolite catalysts. Prevention of deactivation. Optimal conditions for regeneration. *Today* 36: 477-483.
- Behr A, Schüller U, Bauer K, Maschmeyer D, Wiese KD, et al. (2009) Investigations of reasons for the deactivation of rhenium oxide alumina catalyst in the metathesis of pentene-1. *Appl Catal A: General* 357: 34-41.
- Li X, Zhang W, Li X, Liu S, Huang H, et al. (2009) EPR study of the superoxide ion in molybdenum zeolites. *J Phys Chem C* 113: 8228-8233.
- Schalkwyk CV, Spamer A, Moodley DJ, Dube T, Reynhardt J, et al. (2003) Factors that could influence the activity of a WO<sub>3</sub>/SiO<sub>2</sub> catalyst: Part III. *Appl Catal A: General* 255: 143-152.

26. Gangwal SK, Fathi-kalajahi J, Wills GB (1977) Break-in Behavior of a Tungsten Oxide on Silica Catalyst in Propylene Disproportionation. *Ind Eng Chem Prod Res Dev* 16: 237-241.
27. Moodley DJ, Schalkwyk CV, Spamer A, Botha JM, Datye AK (2007) Coke formation on WO<sub>3</sub>/SiO<sub>2</sub> metathesis catalysts. *Appl Catal A: General* 318: 155-159.
28. Mol JC (1997) *Handbook of Heterogeneous Catalysis*. 2nd edition.
29. Siddiqui MRH, Holmes S, He H, Smith W, Coker EN, et al. (2000) Coking and regeneration of palladium-doped H<sub>3</sub>PW<sub>12</sub>O<sub>40</sub>/SiO<sub>2</sub> catalysts. *Catal Lett* 66: 53-57.
30. Khomane RB, Kulkarni BD, Paraskar A, Sainkar SR (2002) Synthesis, characterization and catalytic performance of titanium silicalite-1 prepared in micellar media. *Mater Chem Phys* 76: 99-103.
31. Meng X, Li D, Yang X, Yu Y, Wu S, et al. (2003) Synthesis, Characterization, and Catalytic Activity of Mesoporous Titanosilicates Assembled from Polymer Surfactants with Preformed Titanosilicate Precursors in Strongly Acidic Media. *J Phys Chem B* 107: 8972-8980.
32. Hua D, Chen S-L, Yuan G, Wang Y, Zhao Q, et al. (2011) Metathesis of butene to propene and pentene over WO<sub>3</sub>/MTS-9. *Microporous and Mesoporous Mater* 143: 320-325.
33. Guisnet M, Magnoux P (2001) Organic chemistry of coke formation. *Appl Catal A: General* 212: 83-96.
34. Bibby DM, Howe RF, McLellan GD (1992) Coke formation in high-silica zeolites. *Appl Catal A: General* 93: 1-34.
35. Mellouki A, Liévin J, Herman M (2001) The vibrational spectrum of pyrrole (C<sub>4</sub>H<sub>5</sub>N) and furan (C<sub>4</sub>H<sub>4</sub>O) in the gas phase. *Chem Phys* 271: 239-266.
36. Stepanov AG, Luzgin MV, Arzumanov SS, Ernst H, et al. (2002) *n*-Butene Conversion on H-Ferrierite Studied by <sup>13</sup>C MAS NMR. *J Catal* 211: 165-172.
37. Bigey C, Hilaire L, Maire G (1999) Catalysis on Pd/WO<sub>3</sub> and Pd/WO<sub>2</sub>: Effect of the Modifications of the Surface States Due to Redox Treatments on the Skeletal Rearrangement of Hydrocarbons: Part I. Physical and Chemical Characterizations of Catalysts by BET, TPR, XRD, XAS, and XPS. *J Catal* 184: 406-420.
38. Bartle KD, Ladner WR, Martin TG, Snape CE, et al. (1979) Structural analysis of supercritical-gas extracts of coals. *Fuel* 58: 413-422.
39. Kim DS, Ostromecki M, Wachs IE (1996) Surface structures of supported tungsten oxide catalysts under dehydrated conditions. *J Mol Catal A: Chemical* 106: 93-102.
40. Ramírez J, Gutiérrez-Alejandre A (1997) Characterization and Hydrodesulfurization Activity of W-Based Catalysts Supported on Al<sub>2</sub>O<sub>3</sub>-TiO<sub>2</sub> Mixed Oxides. *J Catal* 170: 108-122.
41. Chua YT, Stair PC (2003) An ultraviolet Raman spectroscopic study of coke formation in methanol to hydrocarbons conversion over zeolite H-MFI. *J Catal* 213: 39-46.
42. Asher SA, Johnson CR (1984) Raman spectroscopy of a coal liquid shows that fluorescence interference is minimized with ultraviolet excitation. *Science* 225: 311-313.